Synthesis of Nanoporous Metal Oxide Particles by a New Inorganic Matrix Spray Pyrolysis Method

S. H. Kim, B. Y. H. Liu, and M. R. Zachariah*

Departments of Mechanical Engineering and Chemistry, Center for NanoEnergetics Research, University of Minnesota, Minneapolis, Minnesota 55455-0111

Received October 11, 2001. Revised Manuscript Received March 27, 2002

In this paper we describe a new approach for the formation of nanoporous particles in which a thermally stable, water-soluble, and therefore easily leached second component is employed during spray pyrolysis to produce a composite particle. We demonstrate the new synthetic approach for synthesizing nanoporous aluminum oxide (Al_2O_3) by spray pyrolysis of aluminum nitrate ($Al(NO_3)_3 \cdot 9H_2O$) and sodium chloride (NaCl) solutions. The characteristics of the nanoporous material such as surface area, pore volume, and particle morphology are investigated as a function of relative humidity, temperature, and salt fractions. Specific surface area of the product particles increased significantly from 10 m^2/g for the produced composite particles to over 370 m^2/g for the remaining Al_2O_3 particles following aqueous leaching to remove the NaCl filler. Nanoporous particles could be produced at relatively low temperature (<550 °C) and high relative humidity (or low evaporation rate of aerosolized droplets) when followed by the aqueous leaching process of final product powder. However, we observed only solid particles at reactor temperatures above 700 °C and residence times of about 1 s. We attribute this behavior to evaporation of salt from the composite particles as evidenced through particles size distribution measurements, which showed the formation of a nuclei mode at these temperatures. At these higher temperatures we suspect a collapse of the porous network in the absence of the supporting salt network and results in particles with low surface area. Intermediate levels of salt fractions result in the formation of nanoporous particles, while high salt fractions result in a loosely connected network and the formation of individual nanoparticles in the salt matrix.

I. Introduction

Microporous inorganic solids such as zeolites have found wide application because of their large internal surface area. However, because of the limitation of pore size to typically <1.5 nm, new synthetic methods have been investigated to extend the range of available pore size. Such methods include using templates of surfactant liquid[1] and colloidal[2] crystals to produce mesoporous materials with pore diameters between 2 and 10 nm. These new methods successfully extend the porosity of zeolite-type materials. Even though they provide opportunities for applications in the fields of molecular sieving and chemical adsorption, they have the disadvantage of requiring a secondary hydrothermal process to remove the surfactant and hence can result in collapse of the pore structure. Furthermore, most templating procedures in batch reactor operations require tediously time-consuming methods, one-time-only use of the templating material, and auxiliary solvent extraction. These latter issues may make many potential applications of these materials uneconomical.

One of the simplest and most industrially viable powder production methods is the spray pyrolysis process. Spray pyrolysis involves the use of one or more precursors dissolved in a solvent and aerosolized into a droplet stream, which is then typically processed in a tubular reactor or flame.[3] Generally, solvent evaporation is accompanied by precursor precipitation and a thermally driven reaction to produce the final product powder. A very wide variety of materials have been produced by this method with single-component and multicomponent metals and metal oxides.[4] One of the easiest approaches to produce metal oxides is to begin with metal nitrate salts, which are readily available, have reasonable solubility in water, and decompose at moderate temperatures (<500 °C). However, to our knowledge, their have been no reports of a process to produce a nanoporous material, although it is quite often observed that conventional spray pyrolysis can lead to hollow particles.[5−7]

Recently, mesoporous silica particles have been produced by a spray pyrolysis method in which polystyrene spheres and surfactants are employed to produce a multiphased self-assembly nanostructure in an evaporating droplet mixed with TEOS ($Si(OCH_2CH_3)_4$), etha-

* To whom correspondence should be addressed. E-mail: mrz@me.umn.edu.

(1) Göltner, C. G.; Antonietti, M. *Adv. Mater.* **1997**, *9* (5), 431.
(2) Velev, O. D.; Jede, T. A.; Lobo, R. F.; Lenhoff, A. M. *Chem. Mater.* **1998**, *10*, 3597.
(3) Zachariah, M. R.; Huzarewicz, S. *J. Mater. Res.* **1991**, *6*, 264.
(4) Kodas, T. T.; Hampdem-Smith, M. J. *Aerosol Processing of Materials*; Wiley−VCH: New York, 1999.
(5) Dubois, B.; Ruffier, D.; Odier, P. *J. Am. Ceram. Soc.* **1989**, *72* (4), 713.
(6) Gadalla, A. M.; Yu, H. F. *J. Mater. Res.* **1990**, *5* (12), 2923.
(7) Senzaki, Y. et al., *J. Am. Ceram. Soc.* **1995**, *78* (1), 2973.

10.1021/cm010957g CCC: $22.00
Published on Web 06/17/2002

nol, and water. However, it has the disadvantage of requiring a secondary thermal calcination process to remove the nanophased additives from the silica/surfactant/polystyrene spheres matrix.[8] Furthermore, the method requires the use of an expensive precursor (polystyrene spheres).

In a related work, nanoparticles have been produced using a salt-assisted spray pyrolysis method. In this approach, molten salt could be used to slow the growth rate down.[9] We have conducted similar experiments in which the salt matrix is generated in situ by the reaction of sodium with metal halides.[10] We have also developed models for coagulating nanoparticles in which the nanopartices are treated as immiscible liquid entities (nanodroplets) within much larger liquid aerosol drops (composed of salt or another liquid medium). We determined that the growth rate and number concentration of nanoparticles in such molten droplets are strongly dependent on the viscosity of the major phase and that since viscosity is highly temperature sensitive, we could employ temperature to change the growth rate of nanoparticles within the liquid drops.[11,12]

In our new approach, we employ salt as a templating medium to support the formation of a nanoporous network. The structure of the network is actually generated during the solvent evaporation phase which solidifies the structure. The particles are then pyrolized as in a traditional spray step to form the metal oxide and permanently freeze in the porous structure. The latter step requires that the spray pyrolysis step be operated below the melting point of salt to ensure that the porous network is undisturbed during the pyrolysis step.

The advantage of the method comes from the simple addition of an inorganic filler. In this experiment, we employ sodium chloride (NaCl) as an inert matrix, which is easily introduced as a second precursor during the preparation of the solution. Salt inclusion offers many advantages. It is inexpensive, readily soluble in water, which makes it easy to produce the initial droplet, thermally stable to quite high temperatures, easily removed from the product particles by aqueous wash, and finally recyclable. We demonstrate the capabilities of this approach by the synthesis of nanoporous alumina which was chosen because it is increasingly being used in adsorption and catalysis where their large surface area, pore structure, and unique surface chemistry play essential roles.[13]

II. Experimental Procedure

Nanoporous alumina was prepared from thermal decomposition of aqueous solution droplets of the metal nitrate and the inorganic filler dissolved at a desired ratio. The precursor solution was prepared by dissolving $Al(NO_3)_3 \cdot 9H_2O$ and NaCl in deionized water with a ratio of 1:5 to 1:1 and a total concentration of 1−3 wt %. A Collison nebulizer was employed with a droplet flow rate of 1 L/min (35 psi). The initial droplet size was measured using a high-sensitivity laser aerosol spectrometer, capable of measuring particle sizes between 65 and 900 nm with a He−Ne optical particle counting system.

In our earliest experiments, we employed a silica gel diffusion dryer right after the nebulizer to remove water from aerosolized droplets. The resulting gas flow through the dryer gave a relative humidity of around 30%. However, because we believe the solidification process is key to the formation of the nanporous network, we modified the experiment to carefully control the drying rate in subsequent experiments. To do this, we controlled the evaporation rate of the aerosolized droplet with a counter-current Nafion membrane dryer. The dryer is constructed with an inner tubular membrane for aerosol flow and outer tube for sheath flow to absorb water vapor. By controlling the relative humidity of the sheath flow, we change the mass-transfer driving force for evaporation. The relative humidity of aerosolized droplets was measured to be 95% at the nebulizer outlet and was varied between 80% RH (low evaporation rate) to a minimum of 50% RH (high evaporation rate), as measured by a relative humidity transducer at the outlet of the Nafion dryer by supplying various ratios of dry/wet air through the outer tube.

The dried solid aerosols were carried to a stainless steel reaction tube (122-cm long, 1.6-cm diameter) within a tube furnace operating at temperatures between 200 and 800 °C as shown in Figure 1. The residence time corrected for temperature ranged from 0.5 s at the highest (800 °C) to 1 s at the lowest (200 °C) temperatures. A differential mobility particle sizer (DMPS)[14] was used to monitor the evolution of particle size distribution at various temperature conditions. The DMPS system is composed of two subsystems: first, a home-built differential mobility analyzer (DMA) classifies singly charged particles by their electrical mobility, and second, a condensation nuclei counter (CNC) counts the particles by growing them via heterogeneous condensation of supersaturated butanol to a size amenable for optical detection. Prior to the DMA, aerosols are exposed to a radioactive source (or neutralizer, Po-210), which generates bipolar ions and produces an equilibrium charge distribution on the aerosols. The mixed Al_2O_3 and NaCl product powder was collected on a nucleopore filter with the powder production rate of 100 mg/h at 25 °C. The nanoporous alumina was obtained after aqueous rinse of the collected product powder.

The product powder was prepared at various temperatures and relative humidity conditions and characterized both before and after aqueous rinse. Powders were characterized by a variety of techniques including scanning electron microscopy (SEM; Model S-900, Hitachi, Ltd.) operated at 8 kV, transmission electron microscopy (TEM; Model JEOL 1210, Hitachi, Ltd.) operated at 100 kV, powder X-ray diffractometry (XRD; Model D-5000, Siemens) using Cu Kα radiation, Fourier transform infrared spectroscopy (FT-IR; Nicolet Series II Magna-IR System 750, Bio-RAD Lab., Inc.), thermal gravimetric analysis (TGA, STA-409, Netzsch, Inc.), and gas sorptometry (BET; ASAP 2000, Micrometrics).

III. Results and Discussion

Since the conversion of nitrate salt to the oxide requires elevated temperature, we needed to make sure that we operate at a temperature below where we would see any appreciable vaporization of salt (or melting of salt at 800 °C). This was determined by generating NaCl aerosols without any of the nitrate and measuring the size distribution with the differential mobility particle sizer (DMPS) system as a function of furnace temperature. As shown in Figure 2, the distribution of NaCl particle remains stable for a temperature below about 550 °C. At 700 °C, the mode corresponding to the

(8) Fan, H. et al., *J. Non-Crystalline Solids* **2001**, *285*, 71.
(9) Xia, B.; Lenggoro, I. W.; Okuyama, K. *Adv. Mater.* **2001**, *13* (20), 1579.
(10) Ehrman, S. H.; Aquino-Class, M. I.; Zachariah, M. R. *J. Mater. Res.* **1999**, *14* (4), 1664.
(11) Struchtrup, H.; Luskin, M.; Zachariah, M. R. *J. Aerosol Sci.* **2001**, *32*, 1479.
(12) Efendiev, Y.; Zachariah, M. R. *Chem. Eng. Sci.* **2001**, *56*, 5763.
(13) Kodas, T. T.; Sood, A. *Alumina Powder Production by Aerosol Processes, Alumina Chemicals: Science and Technology Handbook*; The American Ceramic Society, Inc.: Westerville, OH, 1990.
(14) Fissan, H.; Helsper, C.; Thielen, H. J. *J. Aerosol Sci.* **1983**, *14*, 354.

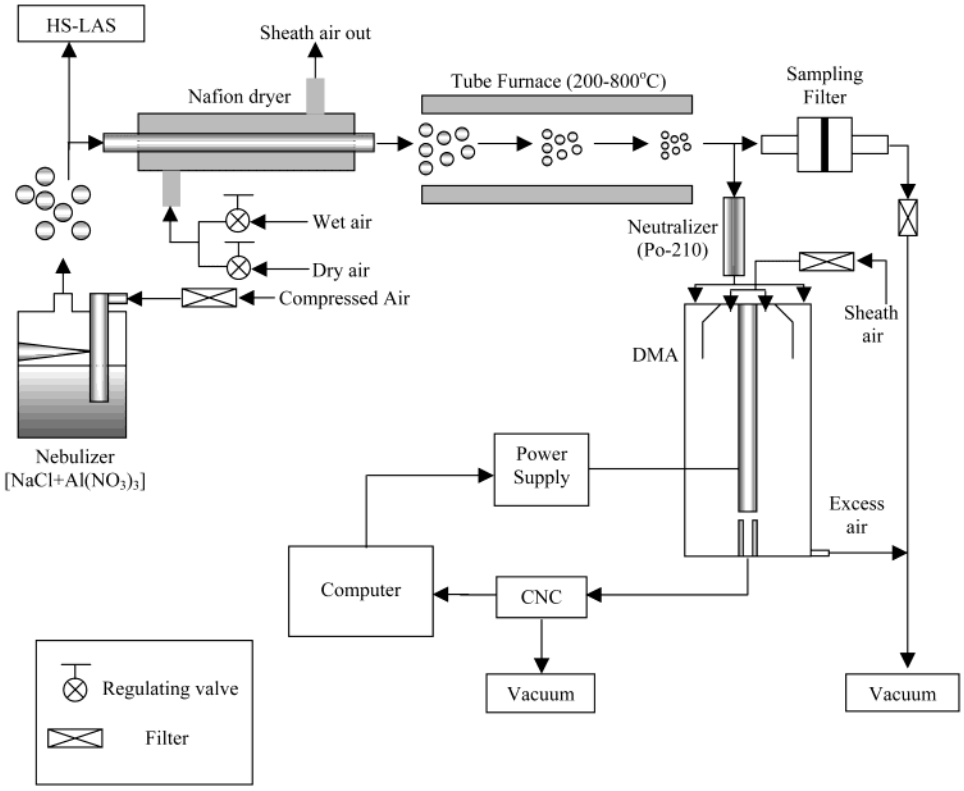

Figure 1. Schematic diagram of the experimental setup for synthesis and characterization of nanoporous particles. (DMA: differential mobility analyzer, CNC: condensation nuclei counter, HS-LAS: high-sensitivity laser aerosol spectrometer).

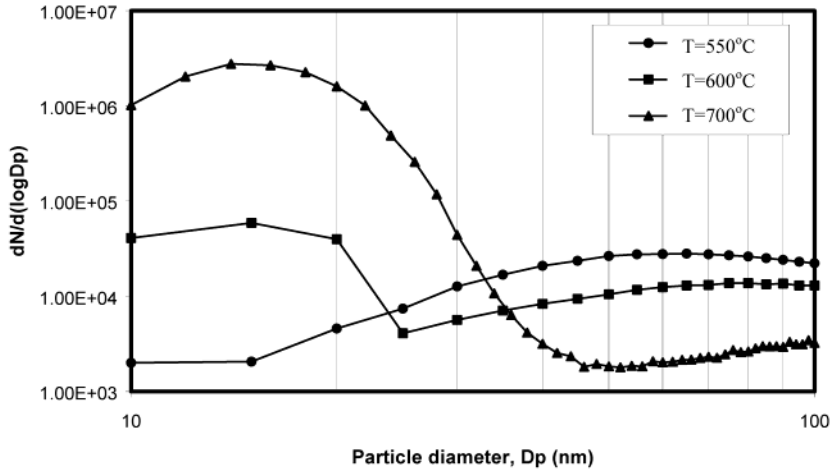

Figure 2. The evolution of NaCl particle size distribution for varying gas temperatures.

original aerosol produced by the atomizer decreases significantly and is replaced with a nucleation mode aerosol with a very narrow size distribution and a high number concentration. On the basis of these results, we maintained the furnace temperatures between 200 and 550 °C, the range where NaCl particles remained stable and $Al(NO_3)_3 \cdot 9H_2O$ is known to thermally decompose. It is known that $Al(NO_3)_3 \cdot 9H_2O$ salt forms a "melt" and releases nitrous oxide gases above 76 °C.[15]

The initial droplet size measured showed that the nominal diameter generated by the nebulizer is about 710 nm as shown in Figure 3. A 1 wt % solution, of a nominally 700-nm droplet should produce a final product particle at full density of about 90 nm. The as-produced particle size distribution for various temper-

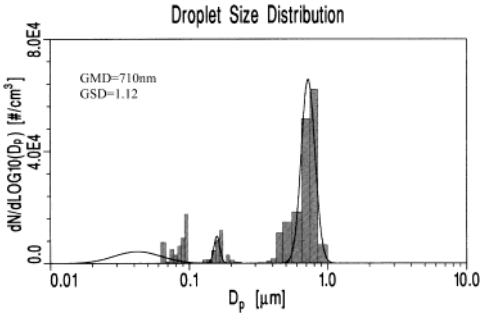

Figure 3. Droplet size distribution from an atomizer (prior to diffusion dryer) measured with a laser aerosol spectrometer. (GMD: geometric mean diameter, GSD: geometric standard deviation).

(15) Cimirelli, R. R., Synthesis of Alumina from Aluminum by Evaporative Decomposition of Solutions, M.S. Thesis, Pennsylvania State University, 1983.

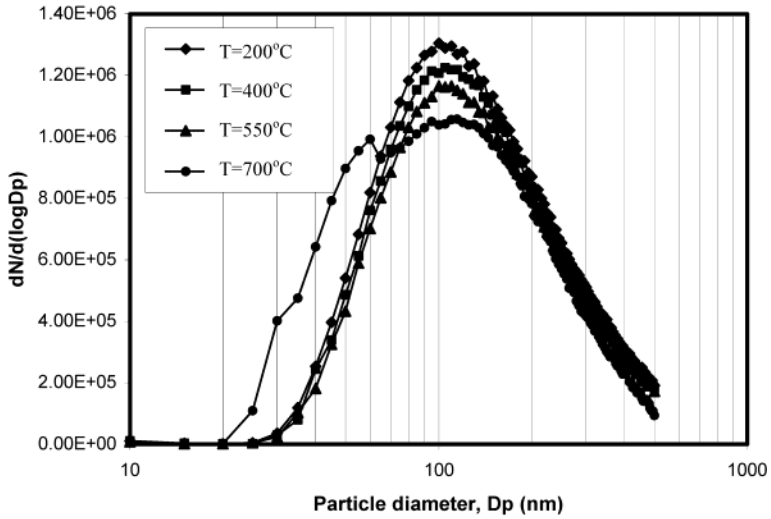

Figure 4. The evolution of final particle size distribution as a function of furnace temperature.

atures as measured by the DMPS is shown in Figure 4. The geometric mean diameter of 100 nm obtained from this measurement is in reasonable agreement with the expected calculated diameter (90 nm), indicating that in general we are not producing hollow particles. We also observe in Figure 4 a decrease in the larger end of the size distribution as we process the particles at higher temperatures and the observation of a smaller mode appearing particularly at 700 °C because of evaporation and re-nucleation of salt, similar to the effect observed and described for pure salt particles (see Figure 2).

In an evaporating droplet, the solute concentration will eventually reach a supersaturated state and begin to nucleate. Since the loss of solvent occurs at the drop surface, it is here that the solute will be at highest concentration. This is moderated because the solute can also diffuse to the interior of the droplet, particularly if the solvent evaporation rate is not too fast. If, however, the evaporation rate is too rapid, then precipitation of the solute near the edge of the droplet can result in the formation of a crust and the potential to subsequently form hollow structures. In our process the nature of the precipitation and its location is intimately connected to the generation of the porous network. The exact nature of the precipitation process is therefore quite complex; however, we expect the salt (36 g/100 g of water) to precipitate first given its lower solubility relative to the nitrate (67 g/100 g of water). As such, one might reasonably expect the outer regions of the particle to have a higher concentration of salt. The extent to which this will occur would depend on the exact nature of the drying rate relative to the internal droplet diffusion processes. Once precipitation is complete, the formation of the porous network is effectively also complete because the solutes are no longer able to move. The only other change that presumably can occur to perturb this network is during the pyrolysis step at elevated temperatures which could cause solid-state or molten-state diffusion to take place.

To verify that indeed we are forming Al_2O_3 particles, Fourier transform infrared spectroscopy (FT-IR) was used. The measured spectra showed strong broad peaks around 700 cm^{-1}, which match very closely the reference spectra for pure Al_2O_3 particles, and indicated that the precursor has been decomposed and converted to alumina under our processing conditions.

X-ray diffraction patterns are shown in Figure 5 for the as-produced and washed powder from a 1 wt % solution of $Al(NO_3)_3 \cdot 9H_2O$ and NaCl with a ratio of 1:1. For the as-produced powder, the spectra show very strong diffraction from salt with a crystallite size estimated using Scherrer's equation[16] of 7 nm (Figure 5a), while after washing one can see the low-intensity broad structure corresponding to alumina with a crystallite size of 4 nm (Figure 5b).

Particle morphology of the Al_2O_3 particles was observed with the use of SEM and TEM. SEM images of the produced composites show spherical, loosely aggregated particles as shown in Figure 6. In general, to produce dense particles by spray pyrolysis, the precipitated precursors should be highly permeable to water vapor and should be processed at a relatively low evaporation rate to ensure the formation of solid (rather than hollow) particles by allowing a more gradual droplet shrinkage process. Following salt removal, some particles, as observed with the SEM, showed hollow shapes (except at 800 °C) and seem to correspond to those that are on the upper end of the particle size distribution (see Figure 4). However, the SEM images taken at 800 °C showed no hollow but highly spherical particles following salt removal presumably because the salt filler completely evaporated and re-nucleated on the outside of the particles.

The TEM images do not show marked differences between the particles with and following salt removal, indicating that salt removal does not significantly alter the overall structure of the particle. Obvious in all images is a thin crust that forms on the outside of the particle presumably as a result of the solvent evaporation process, which leads to the high solute concentration gradient and a fast solutes precipitation at the surface of the droplet. Some slight decrease in the electron beam attenuation is observed in the interior of particles after salt removal has taken place, which indicates that salt did reside within the particle interior. This latter point is corroborated by the fact that the

(16) Guinier, A. *X-Ray Diffraction*; Freeman: San Francisco, 1963; p 124.

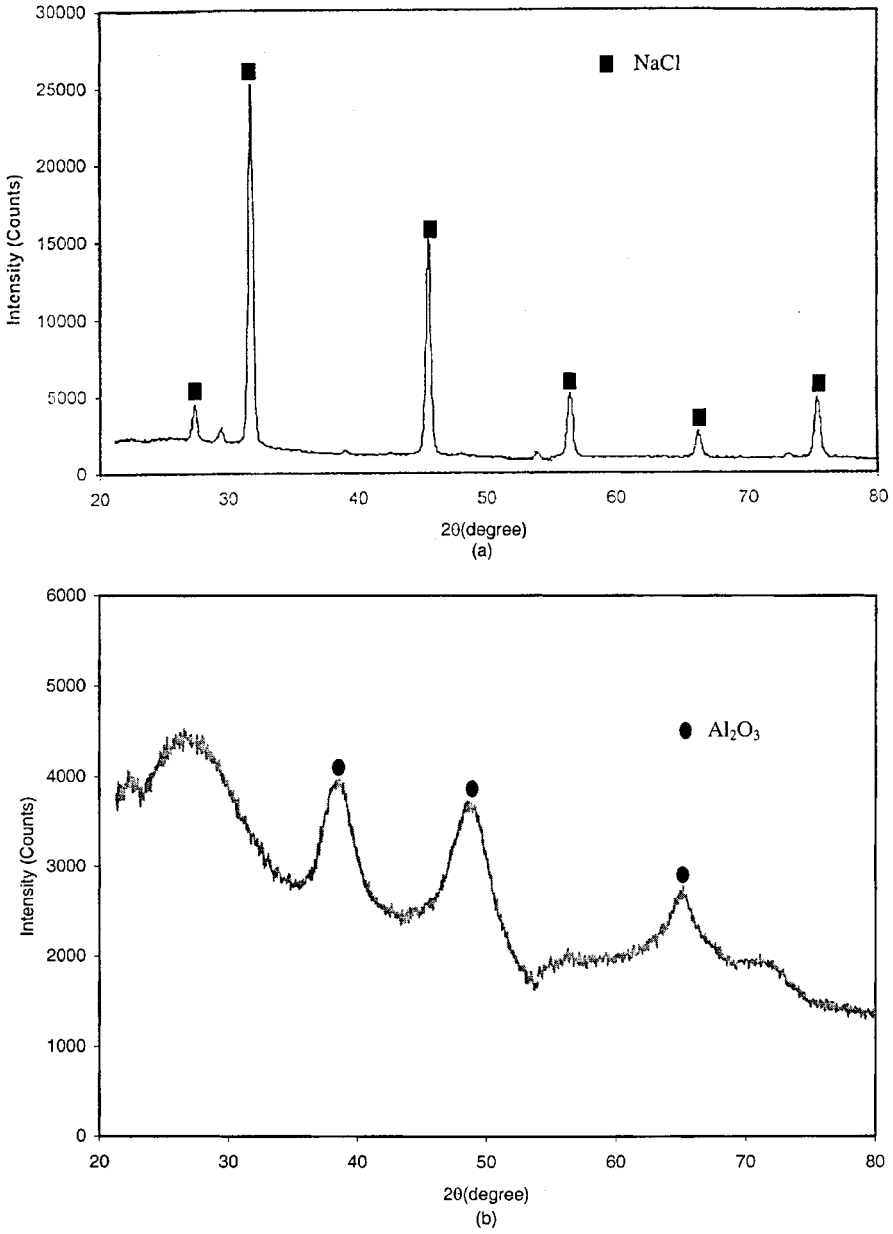

Figure 5. X-ray diffraction patterns of spray-pyrolyzed (a) Al_2O_3 and NaCl (T = 550 °C, before the washing process) and (b) Al_2O_3 particles (T = 550 °C, after the washing process).

e-beam itself causes salt removal and under concentrated electron bombardment can result in salt removal and changes in particle structure. Under normal imaging one focuses the beam optics so as to obtain the sharpest image. In the case of a particle this corresponds to a focal distance where the diameter of the particle is most clearly defined. However, by defocusing the beam so that one is imaging the particle surface, information about surface structure can be inferred, and in our case the porous structure is apparent. The low-temperature case after salt removal shows highly open−broken shell structures as though the only thing that has remained is the thin crust. This presumably is due to the low degree of nitrate conversion to the oxide which upon washing is carried away.

Specific surface area and pore size distribution of the powders were determined by a gas sorptometer (nitrogen adsorption at 77 K using the BET equation) and are summarized in Figure 7. In Figure 7a we see the results for the as-produced particles, which show specific surface areas of only a few square meters per gram, with a near monotonic increase in pore volume with increasing pore diameter. The pore volume increase presumably arises from hollow particles which were observed in the SEM, but which corresponds to a very small surface area. More interesting is the analysis of particles following aqueous leaching of the salt filler as presented in Figure 7b. Pore volume shows a bimodal distribution, with the large mode corresponding to hollow particles and the smaller mode corresponding to the nanoporous structure revealed as a result of removal of the salt filler. Pore surface area shows the most dramatic effects upon removal of the salt filler. We see surface areas are peaking at over 450 m^2/g, which are 2 orders of magnitude higher than the salt-containing powders. Pore size distribution shows that the high surface area corresponds to pore sizes in the 2−10-nm range, which is considerably larger than zeolites. This result shows that the use of the NaCl filler can be used as a crude but highly economical templating medium for producing

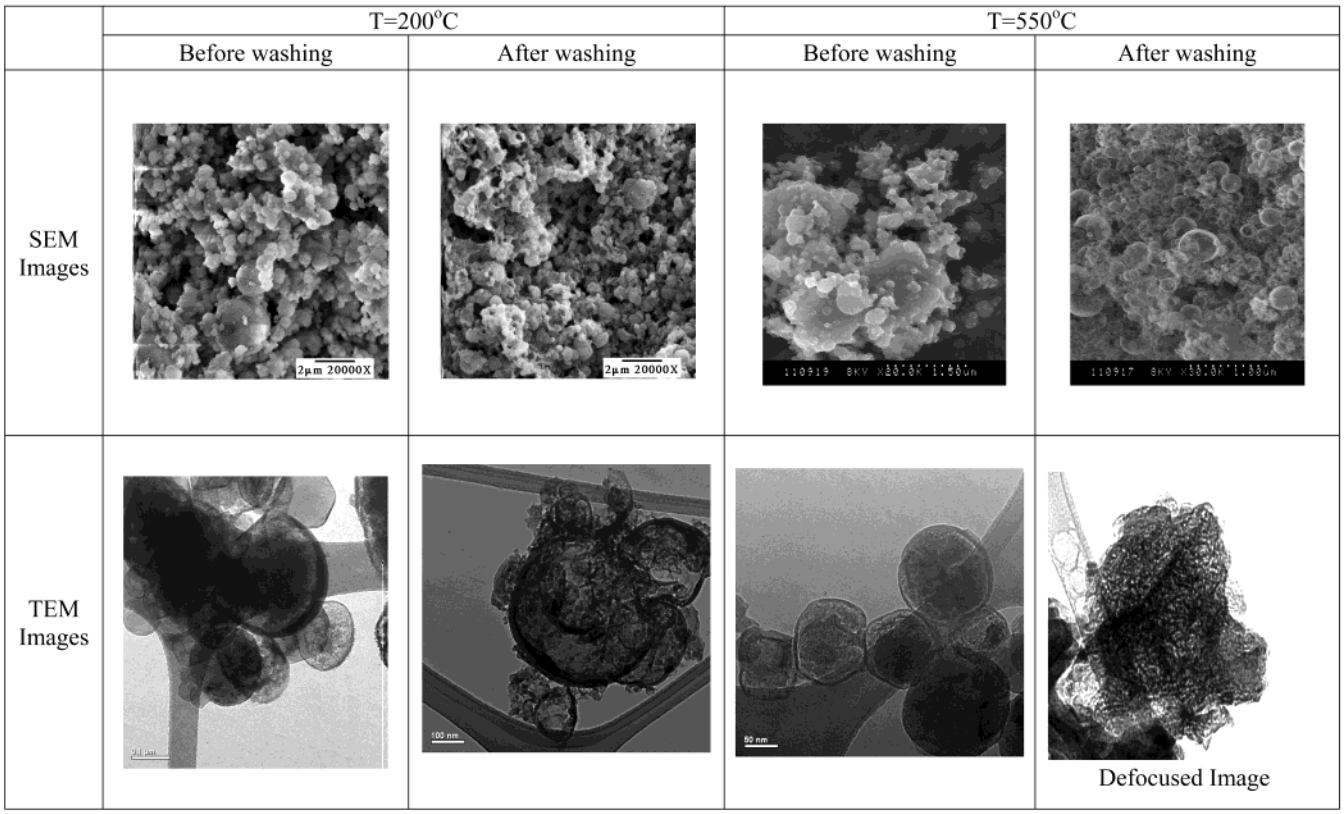

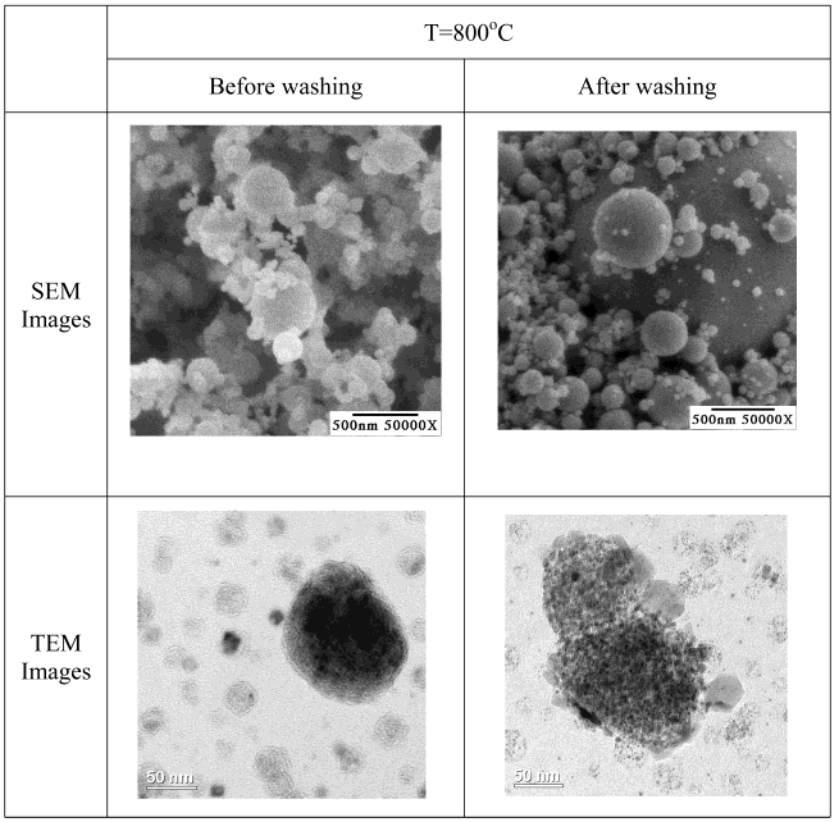

Figure 6. SEM and TEM images for varying temperature and salt content.

nanoporous aerosol particles and that the filler is easily removed through a simple washing procedure.

The effect of processing temperature on total surface area and pore volume is shown in Figure 8a,b, respectively. These results should be placed in context with results for synthesis of pure alumina, which gave a total surface area of 8 and 10 m^2/g at furnace temperatures of 200 and 550 °C, respectively. Results for total surface area following aqueous leaching of salt are shown in Figure 8a. The results show an increase in surface area with increasing temperature to 372 m^2/g (at $T = 550$ °C), followed by a very dramatic decline at higher

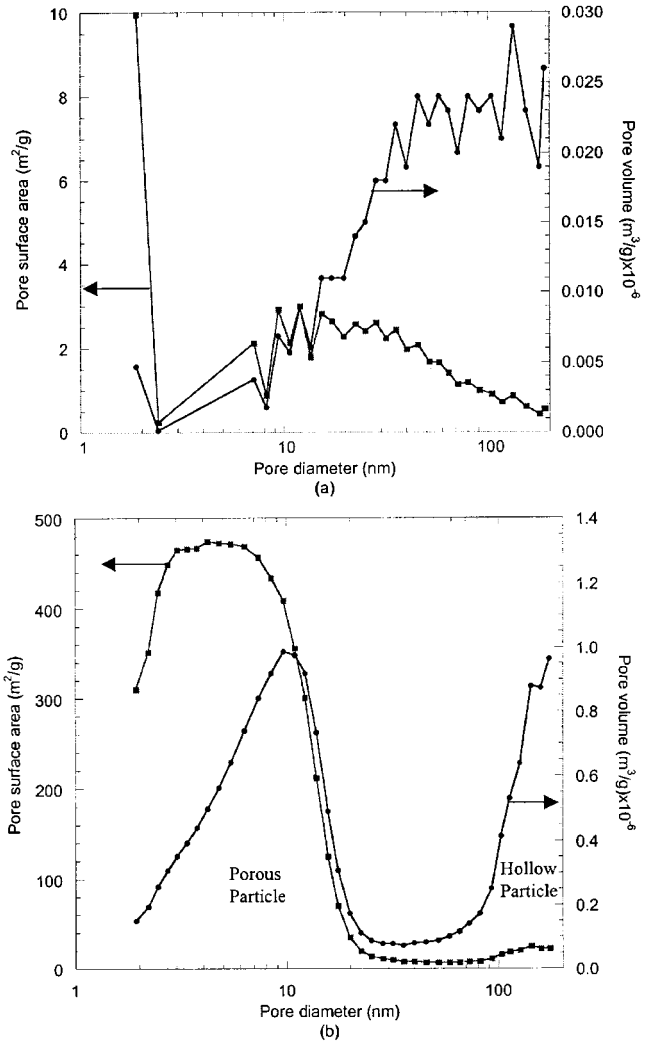

Figure 7. Pore surface area and volume distribution: (a) before and (b) after salt removal ($Al(NO_3)_3$:NaCl = 1:1 at 1 wt % solution, synthesis temperature 550 °C, relative humidity = 30%).

temperatures. One possible explanation for the increase in surface area with increasing temperature (for temperatures below 550 °C) is that incomplete thermal decomposition of aluminum nitrate would result in some of the aluminum content being leached with NaCl during the washing process and result in less particle surface area (per unit mass). This is corroborated by thermal gravimetric analysis of aluminum nitrate as shown in Figure 9. From the calculation of the mass ratio of alumina ($M_{Al_2O_3}$ = 102) to aluminum nitrate ($M_{Al(NO_3)_3\cdot 9H_2O}$ = 375), alumina would be expected to be completely formed at a weight ratio of 27%, which corresponds to 280 °C from the TGA analysis. The TGA results above 400 °C reached a limit of about 20% weight ratio, implying that there is probably more water in the nitrate sample, but more importantly that the decomposition chemistry is complete at temperatures above 400 °C. Our experiments at 200 °C should produce particles that have not completely decomposed as indicated by TGA, which shows a 65% weight ratio. At the higher temperatures the decline in surface area may be associated with the greater atomic mobility of the constituents, which would result, as in any grain growth process, in larger crystallites. Larger crystallites of salt,

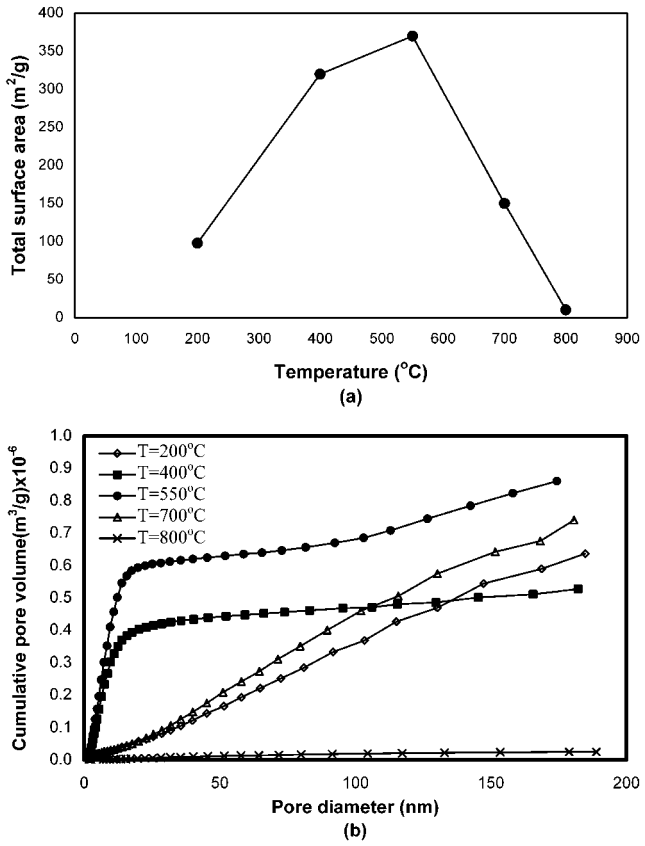

Figure 8. (a) Total pore surface area and (b) pore volume distribution for varying furnace temperatures ($Al(NO_3)_3$:NaCl = 1:1 at 1 wt % solution, relative humidity = 30%, post NaCl removal).

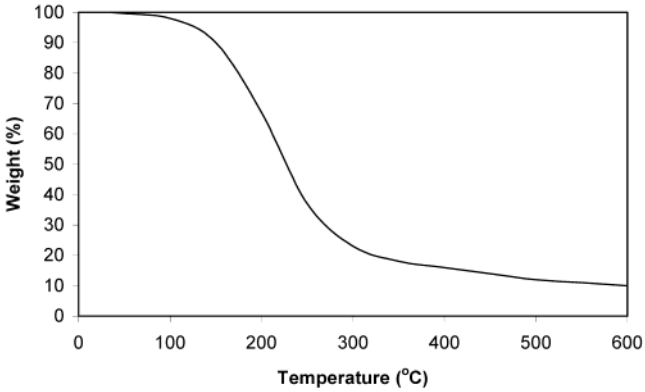

Figure 9. TGA-derived weight loss of aluminum nitrate as a function of temperature.

at the same mass fraction, would lead to a decrease in surface area.

Figure 8b shows the cumulative pore volume at various temperatures. We see that the intermediate temperature cases (400−550 °C) show small pores and moderate pore volume and are indicative of the nanoporous regime of interest. However, as the temperature is increased, we see a decline in the small pore volume and an increase in the overall pore volume (with the exception of the very high temperature 800 °C case). The lowest temperature (200 °C) behavior probably results from incomplete nitrate decomposition as discussed above and, therefore, results in large pores due to loss of aluminum as well as salt. At the higher temperature over 700 °C, we loose salt through evapo-

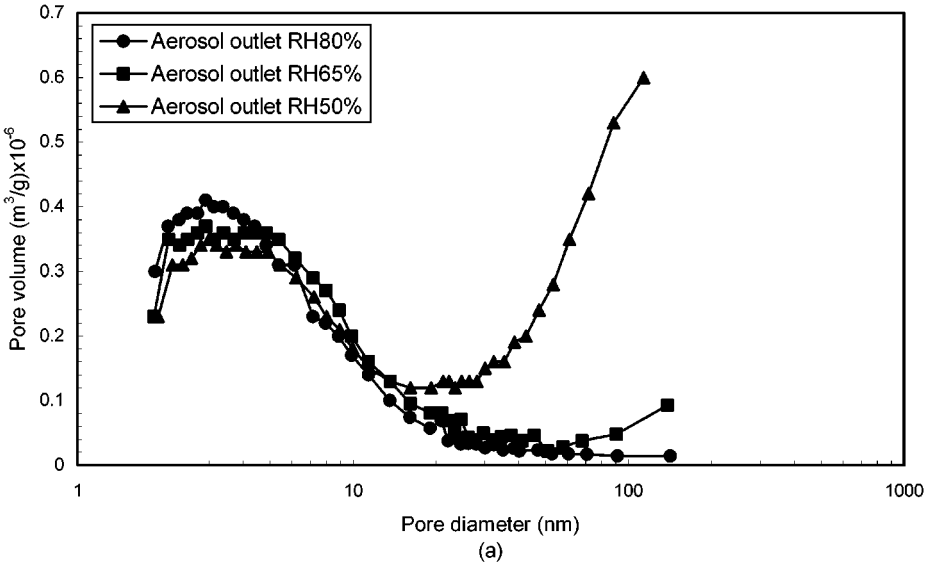

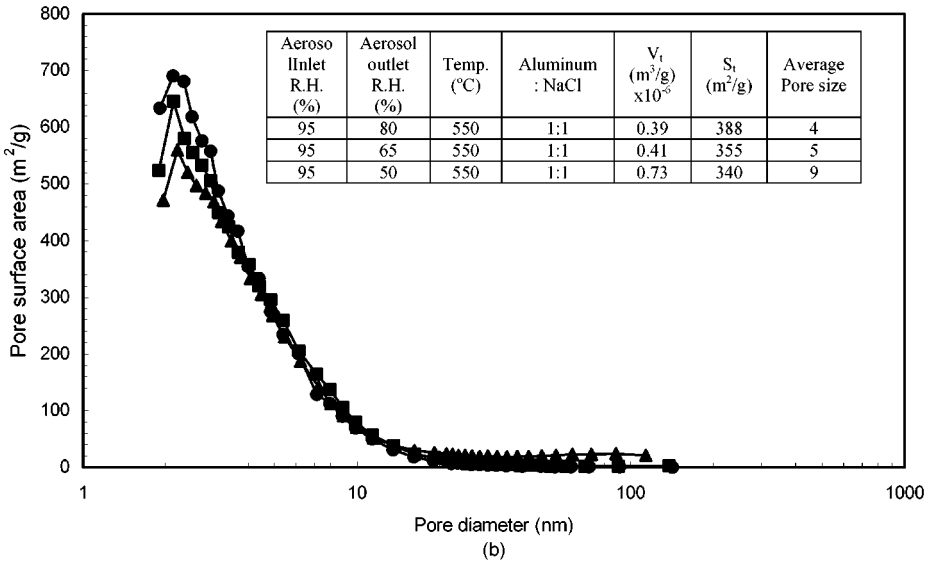

Aeroso lInlet R.H. (%)	Aerosol outlet R.H. (%)	Temp. (°C)	Aluminum : NaCl	V_t (m^3/g) x10^{-6}	S_t (m^2/g)	Average Pore size
95	80	550	1:1	0.39	388	4
95	65	550	1:1	0.41	355	5
95	50	550	1:1	0.73	340	9

Figure 10. The evolution of (a) pore surface area and (b) volume distribution for various drying rate conditions (post salt removal).

ration and hence small pores collapse (see Figures 2 and 4). And at the highest temperature (800 °C) we see a total collapse of the porous or hollow nature of the particle presumably because the salt has melted and therefore cannot preserve the porous network. In summary then, we speculate that the formation of the network is determined by having sufficient thermal energy to convert the nitrate to the oxide, but not so high a temperature as to cause extensive crystal growth of the salt. Finally, at the highest temperatures when the salt melts, we get to the regime discussed in the Introduction whereby we allow the oxide to create its own individual nanoparticles, rather than a porous network.[10]

To investigate the formation of the porous network during the drying process, we varied the evaporation rate by varying the relative humidity of the sheath air in the counter-current Nafion membrane dryer. In Figure 10 we present results for pore volume and pore surface area as a function of drying rate. Higher rates of droplet evaporation result in larger pore sizes. However, the increased average pore sizes at higher droplet evaporation rates are mainly at the higher end of the pore diameter and are associated with the formation of hollow-like structures. On the other hand, there is certainly a trend toward the formation of greater pore volume in the smaller pores (2−10 nm) with decreased drying rate and is qualitatively consistent with our proposed growth mechanism.

The effect of mixture ratio of aluminum nitrate/NaCl is presented in Figure 11. While we have not made any attempts to optimize the fraction of filler needed, we note that increasing the NaCl mass fraction decreases the surface area. With small salt fraction, it is observed that salt filler begins with supporting the porous network inside the composite. With larger salt mass fractions, the resulting composites would presumably have larger salt precipitates and therefore, upon removal of salt, the pore volumes in a small pore size regime (<50 nm) would be decreased and thereby result in decreasing surface area and the formation of alumina nanoparticles similar to our previous works[10] and those of the Okuyama group[9] discussed in the Introduction. From the current experiment, the maximum surface area is around 388 m^2/g at the mixture ratio of aluminum/salt = 1:1 in 1 wt % solution.

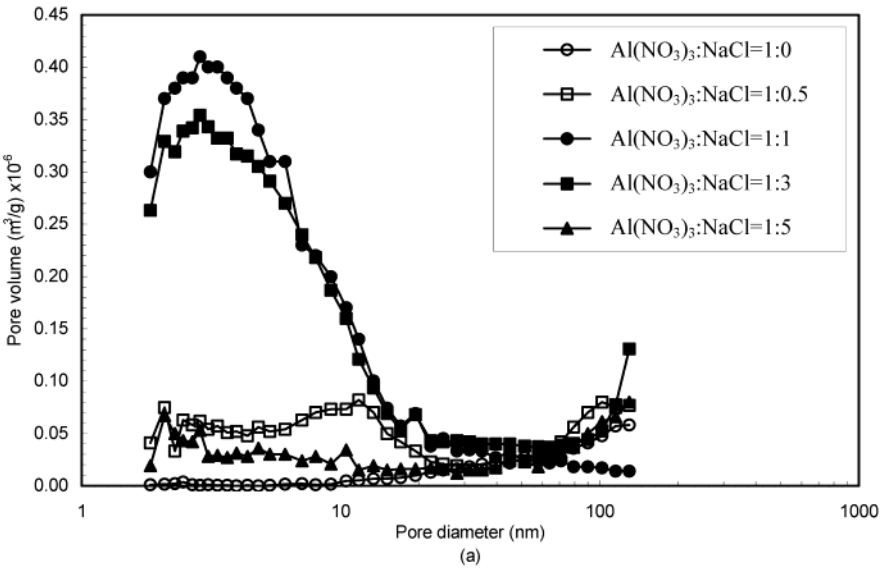

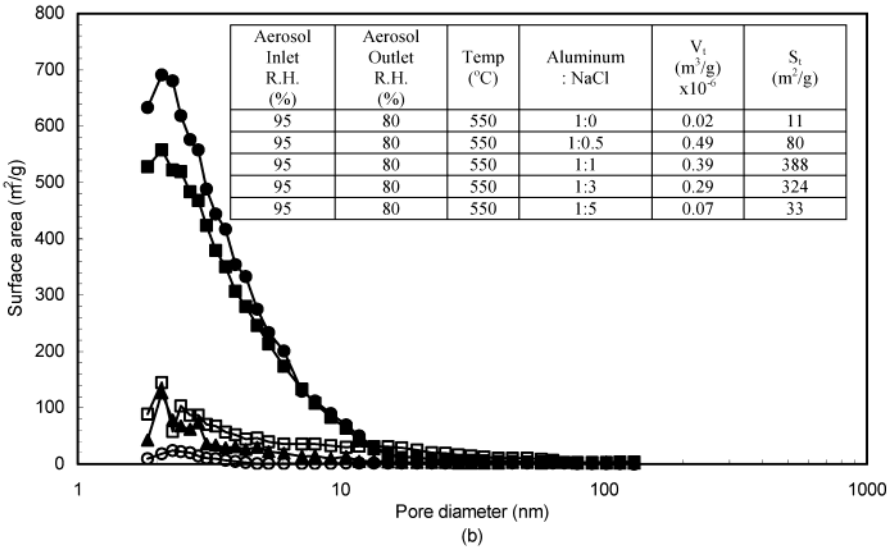

Aerosol Inlet R.H. (%)	Aerosol Outlet R.H. (%)	Temp (°C)	Aluminum : NaCl	V_t (m^3/g) x10^{-6}	S_t (m^2/g)
95	80	550	1:0	0.02	11
95	80	550	1:0.5	0.49	80
95	80	550	1:1	0.39	388
95	80	550	1:3	0.29	324
95	80	550	1:5	0.07	33

Figure 11. The evolution of (a) pore surface area and (b) pore volume distribution of Al_2O_3 for a varying mixture ratio of aluminum and salt (post salt removal).

As discussed in this paper, the evolution of particle morphology is quite sensitive to relative humidity, furnace temperatures, and NaCl filler concentration. The possible processes in the formation of nanoporous Al_2O_3 particles are represented in a simplified schematic diagram in Figure 12. The highly porous dense structures are formed by employing intermediate salt fractions, intermediate temperatures, and high relative humidity conditions. However, we could easily obtain hollow-structured nanoporous particles with intermediate temperature and fast droplet evaporation and point to the fact that it is the drying process that is probably most important in developing the desired morphology. With high salt fractions and intermediate temperatures, the porous structure presumably never forms enough rigidity and can be washed away. If, on the other hand, the processing takes place at high enough temperature and salt factions so that the salt is molten, this allows the alumina fragments to nucleate and grow by internal droplet diffusion, which after washing one obtains nanoparticles as discussed in the Introduction.[10−12] At the high temperatures ($T \geq 700$ °C), for low salt fractions, the molten salt diffuses to the surface and partially evaporates, leaving a densified low-porosity alumina, much the same way traditional spray pyrolysis operates.

The formation of crust, porous, and hollow particles can be thought of as a competition between solute diffusion and solvent evaporation (or droplet shrinkage), which can be evaluated through a comparison of characteristic times[17] presented in Table 1. From Table 1, we see that solute diffusion and droplet shrinkage are clearly the slowest processes among various mechanisms that occurred during spray pyrolysis and that they are sufficiently close to each other that one can consider changing the relative importance of the two mechanisms through changes in process parameters. We compare the relative competition between these processes as shown in Figure 13, where we plot the ratio of the characteristic time of droplet shrinkage (t_r) to that of solute diffusion (t_{sd}) within the droplet as a function of relative humidity. We note that the curve crosses unity at a relative humidity of about 50%, under the

(17) Seinfeld, J. H.; Pandis, S. N. *Atmospheric Chemistry and Physics*; John Wiley & Sons: New York, 1998.

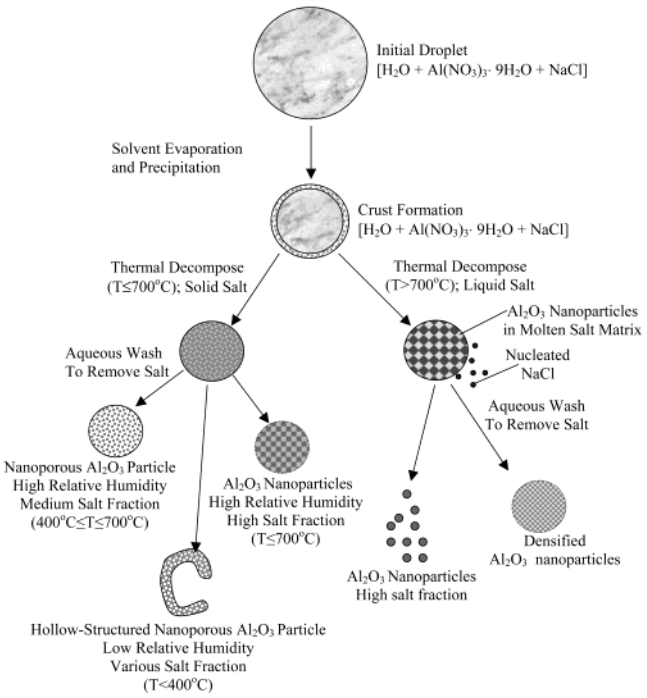

Figure 12. Schematic diagram of the possible processes in the formation of nanoporous Al_2O_3 particles.

Table 1. Comparison of Characteristic Time Constants for Water Droplets Relative to Heat Conduction in Air at $T = 25$ °C

process	characteristic times (s)
vapor diffusion (t_{vd})[a]	2.02×10^{-8}
droplet shrinkage (t_r)[b]	1.69×10^{-4}
solute diffusion (t_{sd})[c]	3.49×10^{-4}
heat conduction in air (t_{hg})[d]	2.23×10^{-7}
heat conduction in droplet (t_{hl})[e]	3.41×10^{-6}

[a] $t_{vd} = d_p^2/D_v$, R = droplet radius (cm), D_v = diffusivity of solvent vapor in air (cm^2 s^{-1}), where R is assumed to be 350 nm, which was measured with a laser spectrometer in this experiment. [b] $t_r = (R_u T \rho_p d_p^2)/(8 D_v M (p_d - p_\infty))$, where ρ_p = density of the liquid phase (g cm^{-3}), R_u = universal constant, D_v = diffusion coefficient of water vapor, M = molecular weight of water, p_d = partial pressure of solvent vapors on the droplet, and p_∞ = partial pressure of solvent vapors far from the droplet. [c] $t_{sd} = d_p^2/D_l$, where D_l = diffusivity of solute in the liquid phase (cm^2 s^{-1}). [d] $t_{hg} = d_p^2/\alpha_g$, where α_g = thermal diffusivity in the gas phase (cm^2 s^{-1}). [e] $t_{hl} = d_p^2/\alpha_l$, where α_l = thermal diffusivity in the liquid phase (cm^2 s^{-1}).

assumption that the vapor pressure of water is unaffected by the solute. At low relative humidity (<50%) the characteristic evaporation time is shorter than the internal droplet transport processes, which should lead to a nonuniform solute profile within the droplet and a corresponding high precipitation rate near the surface. These are the conditions that would lead to a hollow particle, and indeed we observe this under these conditions (see Figure 7b and 10a). At the high relative humidity the ratio of characteristic times is larger than 1 and we observe more uniform porous particles. Of course, we cannot account for salt hydration effects in such simple analysis. Furthermore, initial drop size corresponding to each final particle size could have affected the morphology of the final particle at post-washing due to solubility and the relative diffusion rate of the precursors. Most notably in this regard the formation of hollow particles in the larger final particle size regime (100 nm < D_p < 500 nm) presumably results from incomplete decomposition of the aluminum precursor at the lower temperatures and nonuniform solute distribution at lager particle size, corresponding to larger initial droplet sizes. However, many of the subtle effects observed are not easily explained due to the obviously complex nature of the system.

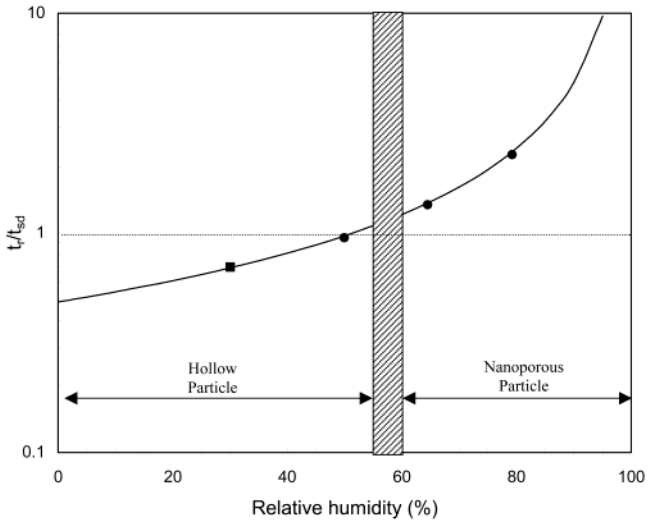

Figure 13. Ratio of characteristic time for droplet shrinkage to solute diffusion, as a function of relative humidity (t_r = characteristic time for droplet shrinkage, t_{sd} = characteristic time for solute diffusion; ● = Nafion membrane dryer, ■ = silica gel diffusion dryer).

IV. Summary and Conclusions

We have demonstrated a new simple method to form nanoporous Al_2O_3 particles by the use of an inorganic filler spray pyrolysis method. The method is shown to provide reasonable control of both particle morphology and porous structure.

Pore sizes in the nanoporous regime ranged from 2 to 20 nm as a result of an aqueous leaching of the NaCl filler. The use of the salt filler requires that aerosol particle processing be limited at temperatures below which significant salt evaporation takes place. We observed that at temperatures of 700 °C and above significant loss of salt resulted in a loss of porosity in the alumina. A large increase in specific surface area of Al_2O_3 particles is observed after washing the NaCl filler from Al_2O_3 and NaCl mixture powder in the temperature range from 400 to 550 °C. Specific surface areas in excess of 370 m^2/g were obtained using the salt filler approach as compared with 10 m^2/g for particles without salt filler. In a high relative humidity environment, highly porous structured particles are produced without the formation of hollow-structured particles due presumably to a reduction of crust formation. Interestingly, the increase of mass fraction of NaCl over the base case (1:1) decreases the specific surface area and enhances the formation of nanoparticles. While we have not addressed this point, we expect, on the basis of these results, that an optimum mixture condition of NaCl/aluminum nitrate exists for a given time/temperature history to produce the desired porosity levels.

This new approach has the advantage of being an economical (low cost and recyclable filler) and control-

lable process for the formation of nanoporous materials on the basis of the future development of this spray pyrolysis method. One should expect that the approach can be extended to a wide variety of material systems with potential applications to catalysis, fillers, thermal barrier coating, and other applications including materials properties enhanced by large surface or void volumes.

Acknowledgment. We gratefully acknowledge the contributions of Dr. Raul Caretta at the University of Minnesota Surface Analysis Center for providing their gas sorptometry measurements. Partial support for this work comes from the Army DURINT Center for Nano-Energetics Research.

CM010957G